NDE DETECTION OF MANUFACTURING DEFECTS IN COMPOSITE BONDED JOINTS USING CFBG SENSORS

Jayanthi Palaniappan [1], Tobias F. Capell [1], Stephen L. Ogin [1], Anthony M. Thorne [1], Andrew D. Crocombe [1], Graham T Reed [1], Swee Chuan Tjin [2], and Lipi Mohanty [2]

[1] Faculty of Engineering and Physical Sciences, University of Surrey, Guildford, GU2 7XH, England
[2] School of Electrical and Electronic Engineering, Photonics Research Centre, Nanyang Technological University, Singapore

ABSTRACT

This paper reports the use of chirped fibre Bragg grating (CFBG) sensors to detect defects introduced during the bonding of composite joints. The single-lap joints were made from transparent GFRP cross-ply composites which had a CFBG sensor embedded within one of the two adherends during the manufacturing stage. Joints with defects simulated using PTFE or introduced real air-gaps have been investigated. The sensors were interrogated with no load on the joints and also under a moderate quasi-static load. For the joints with PTFE "defects", the perturbations observed in the reflected spectra provided a clear indication of the location of the defects and were in very good agreement with modelling predictions. Changes in the reflected spectra for the air-gap defects also provided an indication of the location of the defects and the spectrum changes were in reasonable agreement with modelling predictions. However, further work is required to establish the limitations of the technique for air-gap defects.

1. INTRODUCTION

The increasing use of composite joints has led to the need for an improved understanding of the effect of defects (voids) on joint integrity and for post-bonding inspection methods to verify the integrity of a joint. Early work modelling double-lap bonded joints with voids in the adhesive layers concluded that the voids had little effect on strength, unless a void in the central section of the joint was very large and reduced the remaining bonded area to below that needed to support the applied load [1]. For single-lap joints, where bending is significant, voids in the central section of the bonded area also have a small effect on strength, but voids close to the end of the joint can increase the stresses in the area adjacent to the void by up to 25% [2,3]. The frequency response of a bonded structure is influenced by the presence of voids and disbonds in the adhesive layer, and use of changes in the frequency response has been used to detect weak bonds by examining the damping response of adhesively bonded beams [4,5]. Other techniques used to detect defects in bonded structures include ultrasonics, thermography and some optical methods. Ultrasonic C-scans have been used to detect bonding defects in sandwich structures [6], while thermography has been used to detect bond defects in composite automotive parts [7].

With regard to optical techniques, shearography has been used to detect weak joints and voids [8], and has the advantage that access is required to only one surface of the joint. Chirped fibre Bragg grating (CFBG) sensors, initially used to locate matrix cracking damage in composite materials [9], have also been used to detect defects growing from the end of the overlap of bonded joints as a consequence of fatigue loading [10,11]; this technique does not require access to the joint at all. In addition to monitoring in-service disbond initiation and growth, it would be useful if the embedded CFBG sensors could also detect the presence of defects introduced into the joint during manufacture. Hence, in this work, the use of the CFBG sensors is extended to the detection of defects within the centre of joints introduced during the bonding process.

2. EXPERIMENTAL METHODS

2.1 Composite fabrication

Glass fibre reinforced plastic (GFRP) laminates with embedded CFBGs were manufactured using a wet lay-up process. A steel frame with dimensions approximately 400 mm x 400 mm was wound with dry E-Glass fibre to produce a pre-form having a layup $(0_2/90/0_6)_s$ and nominal ply thickness of 0.25 mm . After the 90^0 ply was wound on the pre-form, two strips of Perspex were bolted to the frame parallel to the 90^0 direction and the optical fibres containing the CFBG sensors were glued to the Perspex using silicon adhesive; the frame was then over-wound with the final 0^0 glass tows. The dry glass fibre perform was impregnated with an epoxy resin matrix system which was composed, by weight, of 100 parts Bisplenol A Epicholorohydrin resin 300, 60 parts MNA hardener and 4 parts Ancamine K61B catalyser. The impregnation was vacuum assisted to fully wet out the pre-form and reduce porosity in the finished laminates (the laminates had a fibre volume fraction of about 0.6). The laminate was cured at 110^o C for 3 hours under a pressure of 0.6 kPa. After fabrication, the laminate was cut into coupons of nominal size 300 mm x 20 mm using a wet diamond saw. Each coupon contained an optical fibre with included CFBG sensor located approximately centrally in the width, within the 0^0 fibres and at the 0/90 interface closest to the outer surface of the laminate. The exact location of the 60 mm sensors along the length of the coupon was established using a hand tightened jig that applied a through-thickness force to the coupon and a perturbation in the reflected spectrum. The coupon was cut so that the low wavelength end of the CFBG was adjacent to the coupon end. The sensors were written on single mode optical fibre and had a full width at the half-maximum of 20 nm, centred at approximately 1540 nm. The portion of the optical fibre containing the sensor had the buffer removed when the grating was written and this was subsequently not replaced, so the cladding of the optical fibre sensor was in direct contact with the epoxy resin matrix in the cured laminates.

The coupon containing the sensor was bonded to a second GFRP coupon (without a sensor), such that the embedded sensor was located approximately 0.5 mm from the bond line. The surfaces were abraded and degreased before being bonded using a one part heat-curing epoxy adhesive, Araldite© AV119. Defects within the bonded joints were simulated in two ways. The first method used a strip of PTFE, 0.25 mm thick, 12 mm long and 20 mm wide. The PTFE "defect" was placed centrally within the length of the joint, creating a sharply-defined defect extending the full width of the joint. Joints manufactured by this method had both adherends 4.5 mm thick (figure 1).

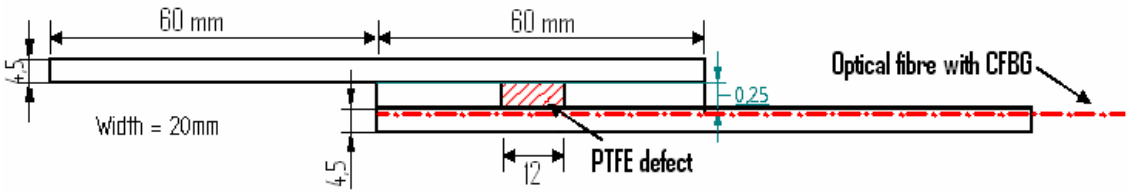

Figure 1: Geometry of bonded joint with PTFE defect.

The second method used selective placement of adhesive to create a full width void within the adhesive layer. Adhesive was applied to the prepared surfaces in such a way as to create a void. Two spacer wires, 0.4 mm thick, were positioned within the adhesive to maintain a constant adhesive thickness in the bonded regions. The joint was

assembled and could be inspected visually (since the GFRP coupons are transparent) to verify that a void (air gap) remained. Joints made by this method used a second adherend either 4.5 mm thick (as before), or a coupon with a lay-up $(0_4/90_2)_s$, which was 3 mm thick (figure 2). Joints prepared using either method were cured for 1 hour at 130^o C while being held together using a spring loaded jig to maintain the correct geometry. Aluminium end tabs were bonded to the finished joints using a two-part structural adhesive, cured at 80^o C for 3 hours. The finished joints were optically transparent, so the location of the defects could be established easily.

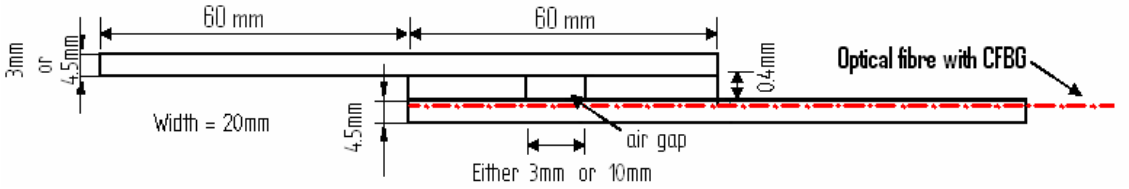

Figure 2: Geometry of bonded joint with air gap defect.

2.2 Testing procedure

The optical arrangement, using a broadband laser and computer controlled optical spectrum analyser (OSA), is shown schematically in figure 3. The bonded joints were clamped into an Instron servo-hydraulic test machine with modified jaws to allow egress of the optical fibre. To establish the effect of a defect on the reflected CFBG spectra, the spectra from the sensor were recorded with no load applied to the joints, and then the joints were loaded statically at a number of discrete load levels. Spectra were compared for the unloaded and loaded cases to detect the defects.

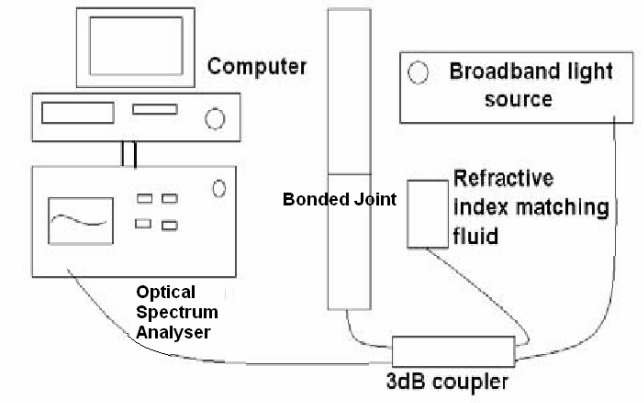

Figure 3: Schematic of the experimental arrangement

3. EXPERIMENTAL RESULTS

3.1 Joints with PTFE “defects”

The reflected spectrum from a CFBG sensor embedded within one adherend of a bonded joint with an included PTFE defect and no external loading is show in figure 4(a). Although slightly noisy, the spectrum shows no indication of any defect within the bonded structure. The PTFE and GFRP adherends have different moduli and coefficients of thermal expansion, but the strain mismatch introduced when cooling the joint to room temperature is not sufficient to be detected within the reflected spectrum. However, when the same joint is loaded to 9 kN load, the reflected spectrum develops perturbations which can be clearly identified.

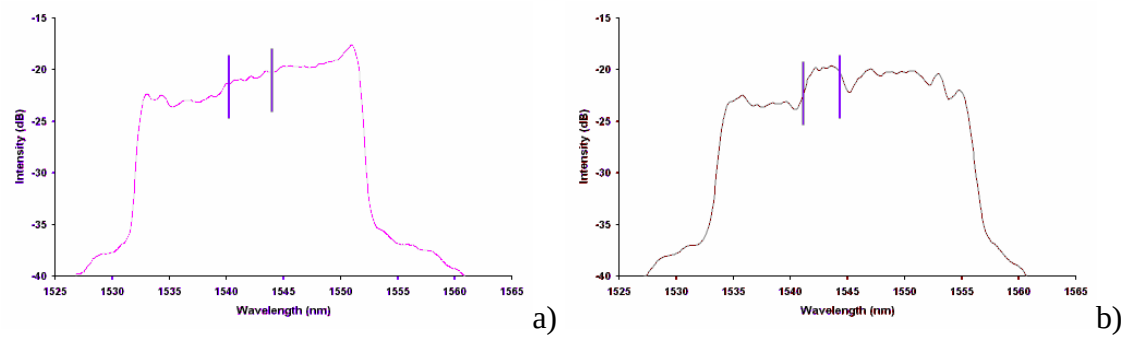

Figure 4: Reflected spectra from bonded joint with 12 mm PTFE defect a) unloaded; b) loaded to 9 kN.

The spectra in figure 4 have been plotted with the addition of vertical lines which show the position of the PTFE defect in the joint in relation to the reflected spectrum. In the unloaded spectrum (figure 4(a)), the vertical lines indicating the defect position are shown based on the physical position at which the defect was introduced into the joint (and can be seen through the transparent adherends) and the fact that the CFBG grating spacing increases linearly for an unloaded joint. Hence, since the mid-point of the defect is positioned at the mid-point of the joint, the defect will also be centred on the mid-point of the reflected spectrum. The situation is slightly more complex for the loaded joint and identifying the position of the defect requires consideration of the non-linearity of the strain distribution (see modelling: Section 4.).

3.2 Joints with air-gap defects

Air-gap defects, made by selectively applying adhesive to the joint to produce the defects, had dimensions parallel to the sensor direction of approximately 3 mm and 10 mm. Figure 5 shows the reflected spectra for a bonded joint with a 3 mm long, full width defect (in this instance the second adherend was 3 mm thick and 30% less stiff than the 4.5 mm coupon). The vertical lines in figure 5(a) show the location of the defect in relation to the reflected spectrum with the joint unloaded, and figure 5(b) shows the relation between the defect position and the spectrum with the joint under a 7 kN load.

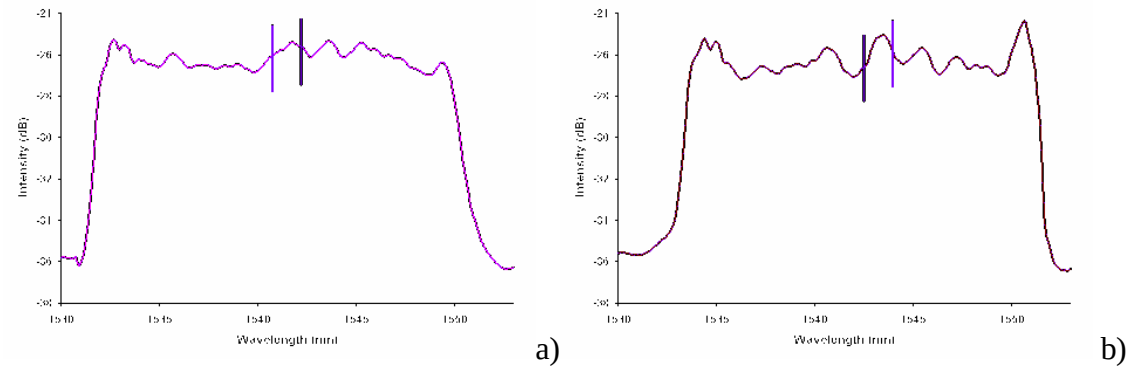

Figure 5: Reflected spectra from bonded joint with 3mm air defect a) under no load b) under 7 kN load.

The reflected spectra for a joint with a 10 mm long air-gap defect are shown in figure 6 (here both adherends were 4.5 mm thick). Again, the spectrum from the unloaded joint is shown (figure 6(a)), and with the joint under a 7 kN load (figure 6(b)). The short vertical lines show the position of the defect relative to the reflected spectrum.

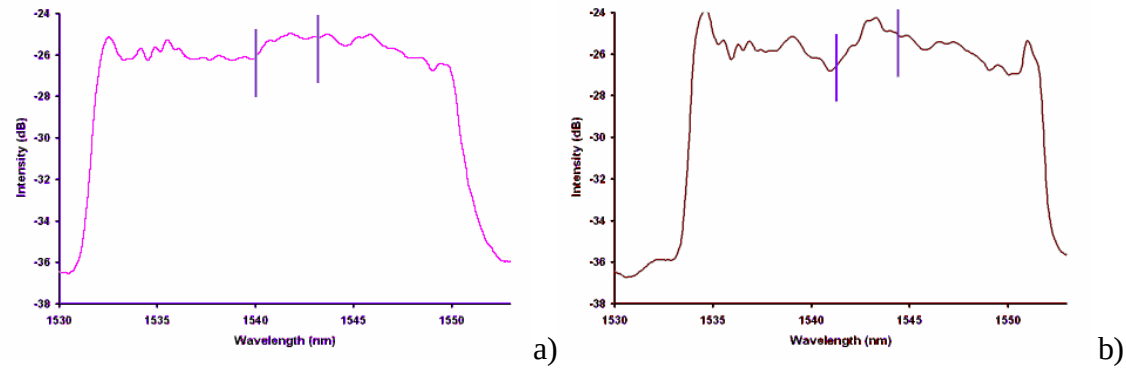

a) b)

Figure 6: Reflected spectra from bonded joint with 10mm air defect a) under no load b) under 7 kN load.

4. PREDICTIONS OF REFLECTED SPECTRA FOR BONDED JOINTS CONTAINING DEFECTS

Bonded joints with defects were modelled using Abaqus© (version 6.6-1 [12]) using two-dimensional models, with the defect represented as a void in the bonded area. The models were created by constructing a one-piece, two-dimensional representation of the bonded joint cross section. The part was then partitioned into the laminate plies and the adhesive layer, with the associated material properties for 0^0 and 90^0 GFRP layers, and AV119 adhesive, being assigned appropriately (the optical fibre was not included explicitly in the model). The model dimensions are as shown in figures 1 and 2. One end of the joint was constrained *encastre* and the other end was constrained to move parallel to the longitudinal direction of the joint, which simulates the loading from the testing machine. On the end surface, a point force was applied to one node which was coupled to other nodes to provide constant displacement in the axial direction. The model was analysed using generalised plane strain and longitudinal strains were extracted from the model corresponding to the position of the core of the optical fibre within the joint; the strain profile along the sensor was converted into a grating spacing and Optigrating© software was used to predict the reflected spectra from the grating spacing [9, 13].

The predicted longitudinal strain profile for a bonded joint with a 12 mm defect (figure 1) under a 9 kN load is shown in figure 7(a). As indicated above, the strain profile is taken along a path which corresponds to the position of the core of the optical fibre in the joint. The position of the 12 mm wide defect within the model is again shown by two vertical lines and the perturbation in the strain field at these points corresponds to the ends of the defect. The predicted spectrum based on this strain profile is shown in figure 7(b), where again, the vertical lines indicate the positions of the defect with respect to the spectrum. The joints with 3 mm and 10 mm air-gap defects, were also modelled in a similar fashion. The strain distributions and predicted spectra are shown in figures 8 and 9.

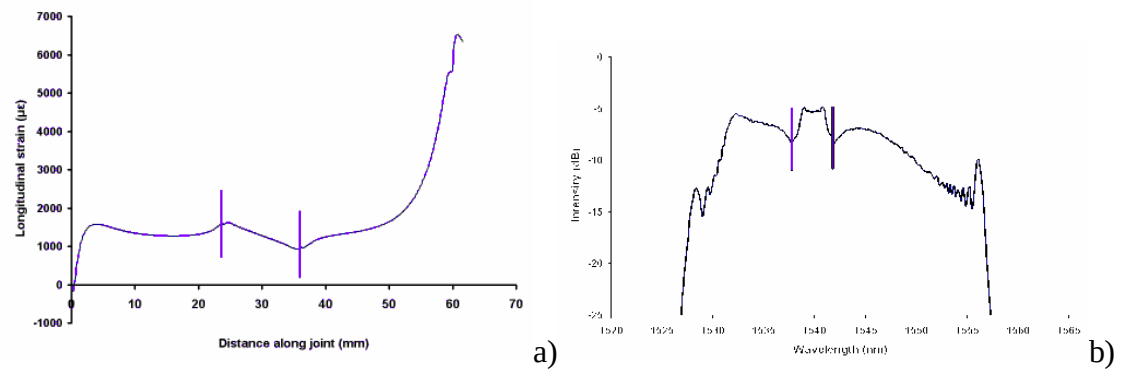

Figure 7: a) Longitudinal strain profile at the position of the core of the optical fibre for a joint with a central 12 mm defect under a 9 kN load. b) Reflected spectrum predicted from this strain profile.

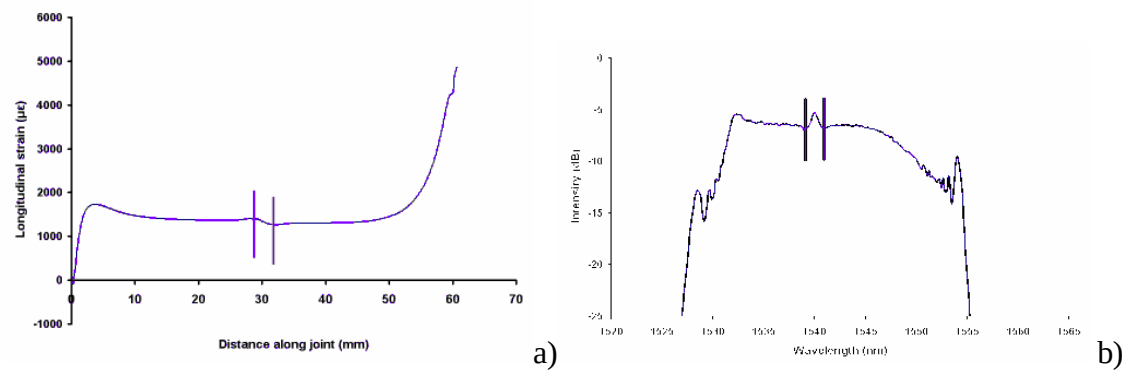

Figure 8: a) Longitudinal strain profile at the position of the core of the optical fibre for a joint with a 3 mm defect under a 7 kN load. b) Reflected spectrum predicted from this strain profile.

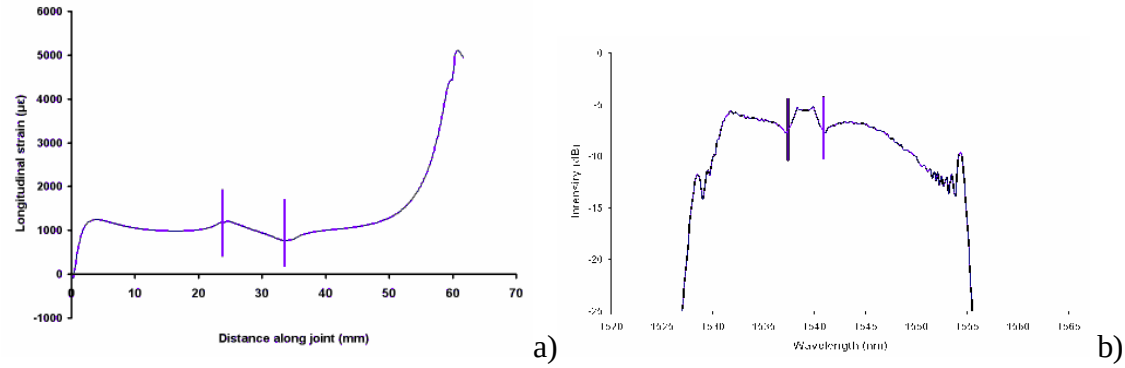

Figure 9: a) Longitudinal strain profile of joint with 10mm defect under a 7 kN load. b) Reflected spectrum predicted from strain profile.

5. DISCUSSION

The experimental results show that defects can be detected within the central portion of bonded joints as a consequence of the changes in the strain distribution which they cause when the joint is under load. The defect can be detected when comparing the reflected spectrum from a loaded and unloaded joint because the sensor is sensitive to the changes in longitudinal strain in the adherends caused by the defects. When a CFBG experiences a constant strain along its length, as is the case in the central portion of a defect-free single-lap joint under load, the reflected spectrum remains the same

shape, but is shifted to higher wavelengths, due to an increase in the grating period caused by the strain. When there is a non-uniform strain due to a defect, the grating period will also change in a non-uniform way. In the case of a joint with a defect under load, the part of the CFBG in the bonded area of the joint will have an increased grating period, but in the region of the defect the rate of increase of grating period will be reduced, because of a reduction in the strain (see figures 7(a), 8(a) and 9 (a)). Some of the grating periods in the sensor adjacent to the defect will then be the same as those in the bonded areas. This increased density of grating periods produces an increase in the intensity of the reflect light, giving a peak in the spectrum for shorter defects (figure 8(b) and a plateau for longer defects (figures 7(b) and 9(b)). The defects simulated using the PTFE had a very well defined geometry and the perturbations in the spectra due to the defect are identifiable clearly in the spectrum, i.e. the two troughs either side of the plateau. The positions of the defect boundaries in the spectrum were measurable to within about 1 or 2 millimetres and the modelling results agree very well with the experimental results.

The modelling predictions for the air-gap defects of 3 mm and 10 mm show a similarly clear result in terms of CFBG spectrum changes for bonds with defects. The experimental results for air-gap defect detection are promising, and changes in the spectra for the bonds with defects are in reasonable agreement with the modelling predictions. However, the current results do not unambiguously demonstrate that the position and extent of the defects could have been deduced from the changes in the spectra alone, and further work is in hand to define the limitations of the technique, using air-gap defects with more carefully defined geometries.

6. CONCLUSIONS

The results have demonstrated the potential for chirped fibre Bragg grating sensors embedded within one adherend of a bonded joint to detect the location of a defect in the joint introduced during manufacture. The position and location of well-defined defects simulated using PTFE have been located unambiguously from the reflection spectra and the results are in very good agreement with modelling predictions. The experimental results from air-gap defects were in reasonable agreement with the predictions, but further work is required to establish the limitations of the technique for detecting air-gap defects.

ACKNOWLEDGEMENTS

The authors would like to thank the University of Surrey and the EPSRC for financial support for JP and TC.

REFERENCES

1- Hart-Smith L.J., “Further developments in the design and analysis of adhesive bonded structural joints.” *Joining of composite materials,* 1981, ASTM STP 749, pp3-31.
2- Olia M. and Rossetos J.N., “Analysis of adhesively bonded joints with gaps subjected to bending.” *Int J Solids Struct,*1996, Vol.33, pp2681–93.
3- de Moura M.F.S.F., Daniaud R. and Magalhaes A.G., “Simulation of mechanical behaviour of composite bonded joints containing strip defects”, *International Journal of Adhesion & Adhesives*, 2006, Vol.26, pp464–473.

4- Yang S., Gibson R.F., Gu L. and Chen W.H., “Modal parameter evaluation of degraded adhesively bonded composite beams.” *Composite structures*, 1998, Vol.43, pp79-91.
5- Yang S., Gu L. and Gibson R.F., “Nondestructive detection of weak joints in adhesively bonded composite structures.” *Composite Structures*, 2001, Vol.51, pp63-71.
6- Hsu D. “Nondestructive testing using air-borne ultrasound”. *Ultrasonics*, 2006, Vol. 44, pp1019-24.
7- Shroeder J., Ahmed T., Chaudry B. and Shepard S. “Non-destructive testing of structural composites and adhesively bonded composite joints: pulsed thermography”, *Composites part A*, 2002, Vol.35, pp1511-7.
8- Pandurangan P. and Buckner G.D., “Defect identification in GRID-LOCK joints.” *NDT&E international*, 2007, Vol.40, pp347-56.
9- Okabe Y., Tsuji R. and Takeda N. “Application of chirped fiber Bragg grating sensors for identification of crack locations in composites”, *Composites Part A*, 2004, Vol. 35, pp59-65.
10- Palaniappan J., Wang H., Ogin S.L., Thorne A.M., Reed G.T., Crocombe A.D. and Tjin S.C. “Structural health monitoring of bonded composite joints using embedded chirped fibre Bragg gratings”, *Advanced Composites Letters*, 2005, Vol. 14/6, pp185-92.
11- Capell T.F., Ogin S.L., Crocombe A.D., Reed G.T., Thorne A.M., Palaniappan J., Tjin S.C. and Mohanty L. *Proceedings of ICCM16*, 2007, Kyoto, Vol. CD, MoBA2-01ge_capellt224232p.
12- ABAQUS by SIMULIA, USA.
13- OptiGrating by Optiwave Corp. Canada.